JACS
JOURNAL OF THE AMERICAN CHEMICAL SOCIETY
Article
pubs.acs.org/JACS

Application of a Mild Hydrothermal Approach Containing an in Situ Reduction Step to the Growth of Single Crystals of the Quaternary U(IV)-Containing Fluorides $Na_4MU_6F_{30}$ (M = Mn^{2+}, Co^{2+}, Ni^{2+}, Cu^{2+}, and Zn^{2+}) Crystal Growth, Structures, and Magnetic Properties

Jeongho Yeon,[†] Mark D. Smith,[†] Joshua Tapp,[‡] Angela Möller,[‡] and Hans-Conrad zur Loye*,[†]

[†]Department of Chemistry and Biochemistry, University of South Carolina, Columbia, South Carolina 29208, United States
[‡]Department of Chemistry and Texas Center for Superconductivity, University of Houston, Houston, Texas 77204, United States

Supporting Information

ABSTRACT: A family of rare U(IV)-containing quaternary fluorides, $Na_4MU_6F_{30}$ (M = Mn^{2+}, Co^{2+}, Ni^{2+}, Cu^{2+}, and Zn^{2+}), was synthesized in single crystal form via a mild hydrothermal technique utilizing an in situ U(VI) to U(IV) reduction step. The modified hydrothermal route is described, and the conditions to obtain single crystals in high yield are detailed. The crystal structures were determined by single crystal X-ray diffraction. The isostructural fluorides crystallize in a new structure type in the trigonal space group $P\bar{3}c1$. They exhibit a complex three-dimensional crystal structure consisting of corner- and edge-shared UF_9 and MF_6 polyhedra. The main building block, a $U_6F_{30}^{6-}$ group, is arranged to create two distinct hexagonal channels, inside which MF_6 octahedra and Na^+ cations are located. The copper-containing member of the series, $Na_4CuU_6F_{30}$, is unusual in that the Cu^{2+} cation exhibits a rare symmetrical coordination environment consisting of six identical Cu−F bond distances, indicating the lack of the expected Jahn−Teller distortion. Magnetic susceptibility measurements of $Na_4ZnU_6F_{30}$ yielded an effective magnetic moment of 3.42 μ_B for the U^{4+} (f^2) cation in the structure. Measurements of the other members containing magnetic transition-metal cations in addition to U^{4+}, $Na_4MU_6F_{30}$ (M = Mn^{2+}, Co^{2+}, Ni^{2+}, and Cu^{2+}) yielded total effective magnetic moments of 10.2, 9.84, 8.87, and 8.52 μ_B for the Mn-, Co-, Ni-, and Cu-containing materials, respectively. No evidence for long-range magnetic ordering was found down to 2 K. Measurements of the magnetization as a function of applied magnetic field at 2 K for $Na_4MnU_6F_{30}$ confirmed that the U^{4+} magnetic cation exhibits a nonmagnetic singlet ground state at low temperature. Thermal stability measurements and UV−vis diffuse reflectance spectroscopy are also reported.

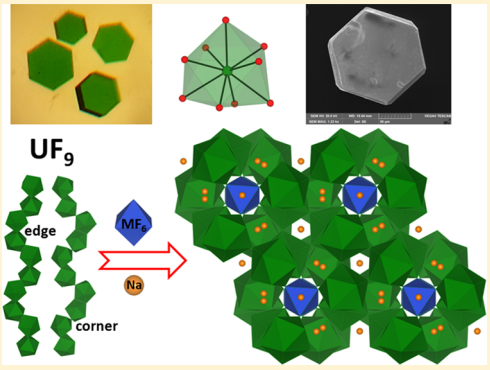

INTRODUCTION

Uranium fluorides are an important group of materials that are fundamental for uranium separation processes, are potential materials for use in long-term nuclear waste storage, and can play a role in the development of new classes of fuel rod assemblies.[1−6] Not surprisingly, the binary uranium fluorides, such as UF_4 and UF_6, have been extensively investigated and are currently being used in a variety of nuclear processes.[7−11] In addition, over 20 ternary inorganic uranium fluorides (other than minerals), such as alkali uranium fluorides and some transition metal uranium fluorides (Na_2UF_6, Na_3UF_7, K_3UF_7, CsU_2F_9, AuU_2F_{11}) have been synthesized, and their structures were reported in the literature.[12−17] Surprisingly, only a handful of quaternary uranium-containing fluorides, such as $CaLi_2UF_8$, have been reported.[18,19] Typically the U^{4+} cations in these structures are found in large coordination environments of UF_x (x = 7, 8, 9) polyhedra that lead to the formation of complex structure types. Remarkably, the total number of transition metal-containing uranium fluorides is very small, considering the importance of uranium as an element. The known uranium fluoride crystal chemistry is dominated by materials containing uranium in the +4 oxidation state, due to the stability of the U^{4+}−F bond. This is quite different from the uranium oxygen chemistry, where uranium is present as U^{6+} and materials mostly contain the ubiquitous uranyl group, UO_2^{2+}, which can direct other coordination environments in the structures and which, sometimes, leads to fluorescent behavior.[20−22] The uranyl chemistry, by comparison with fluorides, has been extensively investigated and many organic−inorganic hybrid materials have been prepared, structurally characterized and reported on in recent years.[23−27] As a result, much more is known about the crystal chemistry of U^{6+}- than of U^{4+}-containing materials.

The dearth of materials containing U^{4+} has motivated us to develop a new synthetic route to prepare U^{4+}-containing materials and to explore their crystal chemistry. Specifically, we have explored the preparation of new uranium-containing

Received: December 18, 2013
Published: March 4, 2014

   dx.doi.org/10.1021/ja412725r | J. Am. Chem. Soc. 2014, 136, 3955−3963

Table 1. Crystallographic Data for $Na_4MU_6F_{30}$ (M = Mn^{2+}, Co^{2+}, Ni^{2+}, Cu^{2+}, and Zn^{2+})

formula	$Na_4MnU_6F_{30}$	$Na_4CoU_6F_{30}$	$Na_4NiU_6F_{30}$	$Na_4CuU_6F_{30}$	$Na_4ZnU_6F_{30}$
fw	2145.08	2149.07	2148.85	2153.68	2155.51
temperature, K	100(2)	100(2)	100(2)	100(2)	100(2)
crystal system	trigonal	trigonal	trigonal	trigonal	trigonal
space group	$P\bar{3}c1$	$P\bar{3}c1$	$P\bar{3}c1$	$P\bar{3}c1$	$P\bar{3}c1$
a (Å)	9.9172(8)	9.8882(3)	9.8623(6)	9.8826(3)	9.8783(7)
c (Å)	13.033(2)	13.015(1)	13.015(2)	13.011(1)	13.046(2)
V (Å^3)	1110.1(2)	1102.09(9)	1096.28(16)	1100.45(8)	1102.4(2)
Z	2	2	2	2	2
density (mg/m^3)	6.418	6.476	6.510	6.500	6.493
absorption coefficient (mm^{-1})	44.471	44.973	45.313	45.252	45.294
crystal size (mm^3)	0.06 × 0.06 × 0.04	0.12 × 0.10 × 0.04	0.10 × 0.08 × 0.05	0.08 × 0.06 × 0.06	0.04 × 0.04 × 0.02
2θ range	4.74–68.64	4.76–70.08	4.76–66.34	4.76–71.26	4.76–69.97
reflections collected	26070	28190	20617	23913	22793
completeness to θ_{max}, %	100.0	100.0	100.0	100.0	100
data/restraints/parameters	1563/0/66	1635/0/66	1404/0/66	1702/0/67	1625/0/66
R (int)	0.0687	0.0565	0.0582	0.0495	0.0815
GOF (F^2)	1.187	1.148	1.161	1.225	1.079
$R(F)^a$	0.0449	0.0304	0.0367	0.0299	0.0361
R_w (F_o^2)^b	0.1089	0.0676	0.0880	0.0702	0.0719
$\Delta\rho$(max/min) (e Å^{-3})	+5.26/−3.80	+6.07/−2.15	+7.77/−2.19	+2.85/−2.56	+5.63/−3.40

$^a R(F) = \sum||F_o| - |F_c||/\sum|F_o|$. $^b R_w(F_o^2) = [\sum w(F_o^2 - F_c^2)^2/\sum w(F_o^2)^2]^{1/2}$.

fluorides and have developed a mild hydrothermal synthetic approach for the preparation of extended U^{4+}-containing fluoride structures. We are particularly interested in materials containing reduced uranium cations, because not only do they give rise to new complex crystal structures due to the large size of the U^{4+} cation but also such materials can exhibit interesting magnetic properties due to the presence of unpaired f-electrons in the U^{4+} (f^2) cation.[28−31]

In our recent studies, we reported on two general synthetic approaches to produce U^{4+}, including the use of U^{4+}-containing precursors, such as $U(C_2O_4)_2(H_2O)_6$ and the in situ creation of U^{4+} from U^{6+}-containing precursors, such as $UO_2(CH_3CO_2)_2\cdot 2H_2O$.[32,33] While a variety of organic species, such as polyols, oxalic acid, and acetate, can function as reducing agents to prepare U^{4+}-containing precursors,[34−37] the application of uranium acetate for the mild hydrothermal in situ preparation of U^{4+} combines being a uranium source with the acetate species as a reducing agent, thereby eliminating the need to synthesize U^{4+}-containing precursors. Using this method, we previously communicated the synthesis of $U_3F_{12}(H_2O)$, a new U^{4+}-based uranium fluoride.[33] In this paper we report on our significant breakthrough in using this mild hydrothermal method to prepare a new series of quaternary transition metal-containing uranium fluorides, $Na_4MU_6F_{30}$ (M = Mn^{2+}, Co^{2+}, Ni^{2+}, Cu^{2+}, and Zn^{2+}), representing a significant expansion of known quaternary uranium fluorides. The synthesis, crystal structures, and magnetic properties of this series of U^{4+}-containing quaternary fluorides are discussed within.

EXPERIMENTAL SECTION

Reagents. $UO_2(CH_3CO_2)_2\cdot 2H_2O$ (International Bio-Analytical Industries Inc., ACS grade), NaF (Alfa Aesar, 99%), $MnCl_2\cdot 4H_2O$ (Alfa Aesar, 99%), $CoCl_2\cdot 6H_2O$ (J.T. Baker, 99+%), $NiCl_2\cdot 6H_2O$ (Aldrich, 99%), $Cu(CH_3CO_2)_2\cdot 2H_2O$ (Aldrich, 98+%), $ZnCl_2$ (Alfa Aesar, 98+%), and HF (Alfa Aesar, 48%) were used as received. Warning: although the uranium precursors used contain depleted uranium, standard safety measures for handling radioactive substance should be followed. HF should only be handled in a well ventilated space and care should be taken to use proper safety precautions.

Synthesis. Single crystals of the title compounds were grown using a mild hydrothermal route incorporating a U(VI) to U(IV) reduction step. Specifically, for the preparation of $Na_4MU_6F_{30}$ (M = Mn^{2+}, Co^{2+}, Ni^{2+}, Cu^{2+}, and Zn^{2+}), 2 mmol of $UO_2(CH_3CO_2)_2\cdot 2H_2O$, 2 mmol of NaF, 1 mL of H_2O, and 2 mL of HF (18.4 M) were combined with 8 mmol of $MnCl_2\cdot 4H_2O$, $CoCl_2\cdot 6H_2O$, $NiCl_2\cdot 6H_2O$, and $ZnCl_2$, respectively. For the preparation of $Na_4CuU_6F_{30}$, 1 mmol of $UO_2(CH_3CO_2)_2\cdot 2H_2O$, 1 mmol of NaF, 1 mL of H_2O, and 1 mL of HF (12.8 M) were combined with 1 mmol of $Cu(CH_3CO_2)_2\cdot 2H_2O$.

The respective solutions were placed into 23 mL Teflon-lined autoclaves. The autoclaves were closed, heated to 200 °C at a rate of 5 °C min^{-1}, held for 1 day, and cooled to room temperature at a rate of 6 °C h^{-1}. The mother liquor was decanted from the single crystal products, which were isolated by filtration and washed with distilled water and acetone. In all cases except $Na_4CuU_6F_{30}$, the reaction yielded a single phase product consisting of light-green hexagonal plate crystals in approximately 20%, 70%, 60%, and 80% yields for Mn-, Co-, Ni-, and Zn-containing materials based on $UO_2(CH_3CO_2)_2\cdot 2H_2O$. For $Na_4CuU_6F_{30}$, green crystals were obtained in a nearly quantitative yield based on $UO_2(CH_3CO_2)_2\cdot 2H_2O$, along with Cu metal powder that was selectively removed by dissolving it in concentrated HNO_3. As seen in Figure S1, the PXRD patterns on the ground crystals indicate that no impurities are contained in the products.

Single Crystal X-ray Diffraction. X-ray intensity data from light-green hexagonal plates were collected at 100(2) K using a Bruker SMART APEX diffractometer (Mo Kα radiation, 0.71073 Å).[38] The data collections covered 100% of reciprocal space to limiting $2\theta_{max}$ values of 68.6–71.3°, with R_{int} = 0.050–0.069 after absorption correction. The raw area detector data frames were reduced and corrected for absorption effects with the SAINT+ and SADABS programs.[38] Final unit cell parameters were determined by least-squares refinement of large sets of strong reflections taken from the data sets. Direct methods of structure solution, difference Fourier calculations, and full-matrix least-squares refinement against F^2 were performed with SHELXS/L as implemented in OLEX2.[39,40]

The compounds crystallize in the trigonal system. Systematic absences in the intensity data were consistent with a c-glide symmetry element perpendicular to [100], leaving $P3c1$ and $P\bar{3}c1$ as space group choices. The centrosymmetric group $P\bar{3}c1$ was confirmed by obtaining a sensible and stable refinement of the structure. The asymmetric unit

Table 2. Selected Interatomic Distances (Å) for $Na_4MU_6F_{30}$ (M = Mn^{2+}, Co^{2+}, Ni^{2+}, Cu^{2+}, and Zn^{2+})

	$Na_4MnU_6F_{30}$	$Na_4CoU_6F_{30}$	$Na_4NiU_6F_{30}$	$Na_4CuU_6F_{30}$	$Na_4ZnU_6F_{30}$
U(1)−F(4)	2.226(6)	2.240(4)	2.249(5)	2.250(4)	2.245(4)
U(1)−F(2)	2.269(5)	2.264(3)	2.262(5)	2.268(3)	2.263(4)
U(1)−F(5)	2.300(5)	2.298(4)	2.299(5)	2.298(3)	2.298(4)
U(1)−F(3)	2.307(5)	2.316(4)	2.317(5)	2.314(3)	2.316(4)
U(1)−F(1)	2.324(5)	2.326(4)	2.320(5)	2.323(3)	2.321(4)
U(1)−F(5)	2.342(5)	2.335(4)	2.334(5)	2.340(3)	2.337(4)
U(1)−F(2)	2.360(5)	2.355(4)	2.349(5)	2.345(3)	2.352(4)
U(1)−F(3)	2.412(5)	2.421(4)	2.422(5)	2.418(3)	2.428(4)
U(1)−F(1)	2.426(5)	2.418(4)	2.420(5)	2.415(3)	2.425(4)
M(1)-F(4)	2.056(5) × 6	2.013(4) × 6	1.986(5) × 6	1.995(4) × 6	1.996(4) × 6

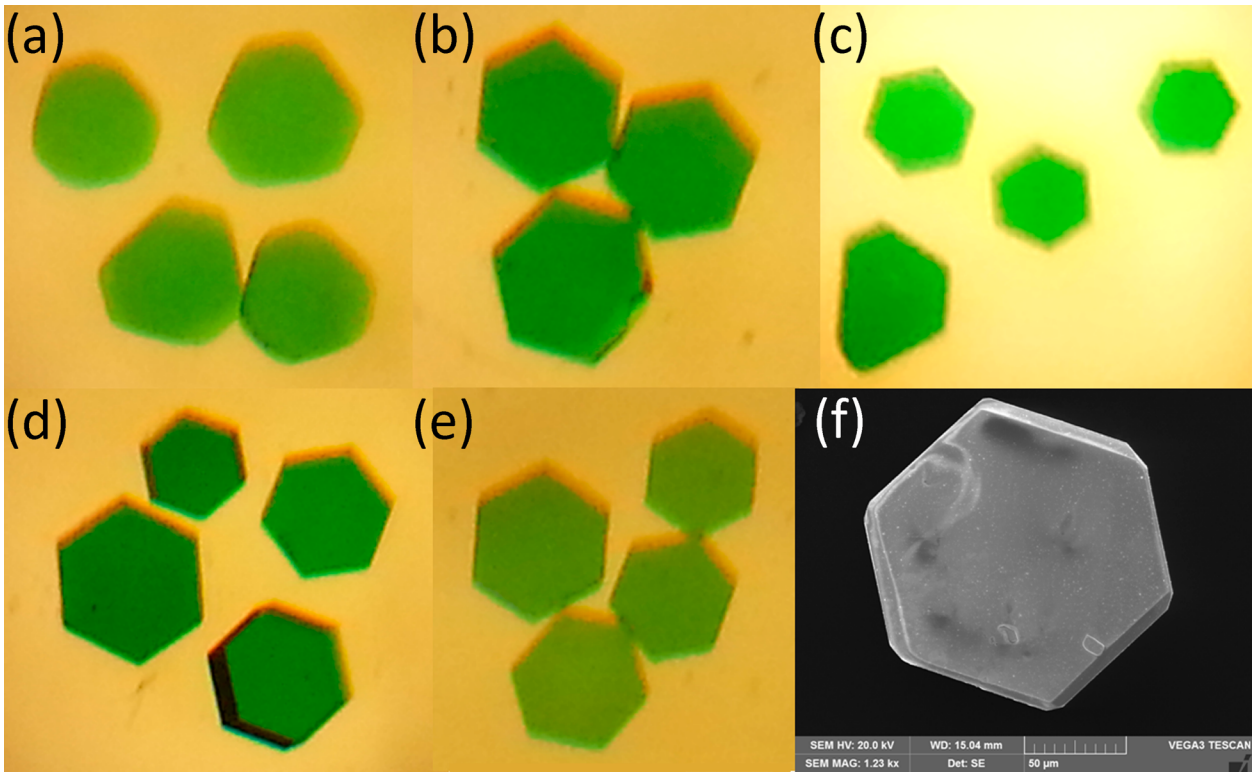

Figure 1. Optical images of single crystal for (a) $Na_4MnU_6F_{30}$, (b) $Na_4CoU_6F_{30}$, (c) $Na_4NiU_6F_{30}$, (d) $Na_4CuU_6F_{30}$, and (e) $Na_4ZnU_6F_{30}$, and (f) a SEM image of a single crystal of $Na_4CuU_6F_{30}$.

consists of one uranium, one divalent transition metal, three sodium, and five fluoride atomic positions. The uranium atom U(1) and all five fluoride atoms are located on general positions (Wyckoff symbol 12*g*). The divalent atoms are located on position 2*a*, with (32) site symmetry. Sodium atom Na(1) is located on a 3-fold axis (position 4*d*). Na(2) is located on site 2*b*, with (3) site symmetry. After location and refinement of the four metal and five fluoride atomic positions described above, a residual electron density peak of ∼5 $e^-/Å^3$ was observed in a roughly ellipsoidal cavity. The cavity is bounded by fluoride atoms with distances of 2.3−2.7 Å from the cavity center, i.e., a chemically feasible location. This peak was modeled as the third unique sodium site, Na(3). The observed electron density concentration is displaced by ∼0.5 Å from the center of the cavity, over two symmetry-equivalent sites related by a two-fold axis (Figure S2). Refinement as a half-occupied sodium resulted in a senselessly large displacement parameter. Refinement of the Na(3) site occupancy factor (sof) yielded an occupancy value near 1/6 and an acceptable displacement parameter. This occupancy value also produces a stoichiometry within experimental error of electroneutrality. Na(3) therefore occupies a split and partially occupied position, disordered about a two-fold axis of rotation (position 6f). For the final refinement, the Na(3) sof was fixed at 1/6. Refinements of the site occupancies of the other metal sites showed no significant deviations from full occupancy. All atoms were refined with anisotropic displacement parameters except for the disordered and 1/6-occupied atom Na(3) (isotropic). The largest residual electron density peaks in the final difference maps are located <1 Å from the uranium atom in each data set. Crystallographic data, selected interatomic distances, and atomic coordinates are listed in Tables 1, 2, and S1, respectively.

Powder X-ray Diffraction. PXRD data were collected on a Rigaku D/Max-2100 powder X-ray diffractometer using Cu Kα radiation. The step-scan covered the angular range 10−80° 2θ in steps of 0.04°. No impurities were observed, and the calculated and experimental PXRD patterns are in excellent agreement (see Figure S1).

UV−vis Diffuse Reflectance Spectroscopy. Diffuse reflectance spectra of polycrystalline powder samples of the reported materials were obtained using a Perkin-Elmer Lambda 35 UV−vis scanning spectrophotometer equipped with an integrating sphere over the range of 200−900 nm. Reflectance data were converted to absorbance using the Kubelka−Munk function.[41]

Electron Paramagnetic Resonance (EPR) Spectroscopy. Room-temperature X-band (9.38 GHz) EPR spectrum was collected

dx.doi.org/10.1021/ja412725r | J. Am. Chem. Soc. 2014, 136, 3955−3963

on a powdered sample (~430 mg) for $Na_4CuU_6F_{30}$ packed in a quartz tube using a Bruker EMX plus spectrometer with 20 mW microwave power and a modulation amplitude of 10 G.

Scanning Electron Microscopy. Scanning electron micrographs of the single crystals of $Na_4MU_6F_{30}$ were obtained using a Tescan Vega-3 SEM instrument utilized in low-vacuum mode. A SEM image of a representative crystal of $Na_4CuU_6F_{30}$ is shown in Figure 1. Energy dispersive spectroscopy (EDS) using a Thermo EDS instrument also verified the presence of uranium, the respective divalent transition metal, sodium, and fluorine in $Na_4MU_6F_{30}$ (M = Mn^{2+}, Co^{2+}, Ni^{2+}, Cu^{2+}, and Zn^{2+}).

Magnetic Property Measurements. The magnetic properties of the microcrystalline compounds were measured using a Quantum Design Physical Property Measurement System (QD-PPMS) equipped with a vibrating sample magnetometer. Temperature-dependent susceptibility measurements were made in both zero-field cooled (ZFC) and field cooled (FC) conditions in applied fields of 1000 Oe. Magnetization measurements at 2 K were carried out in applied fields up to 8 T.

RESULTS AND DISCUSSION

Synthesis. We utilized a mild hydrothermal technique at the relatively low temperature of 200 °C and synthesized a series of new U^{4+}-containing quaternary fluorides, $Na_4MU_6F_{30}$ (M = Mn^{2+}, Co^{2+}, Ni^{2+}, Cu^{2+}, and Zn^{2+}), that crystallize in a new structure type. The U^{6+} cation in the starting reagent, $UO_2(CH_3CO_2)_2{\cdot}2H_2O$, was successfully reduced to U^{4+} during the synthesis in a dilute hydrofluoric acid environment. The product yield is generally very high for this synthetic approach, and, for example, the Cu analogue crystallized in a nearly quantitative yield. The X-ray powder patterns collected using ground crystals match perfectly with the powder diffraction patterns calculated using the single crystal data, as shown in Figure S1. The reaction only generated the title phases as high-quality single crystals, and no secondary phases were observed. The crystal morphology for all compositions was identical, and representative optical and SEM images of the green, hexagonal crystals are shown in Figure 1. The synthesis of the iron analog, in spite of numerous attempts to obtain it, always resulted in a related but different series of quaternary fluorides containing +3 metal cations, whose structures and magnetic properties will be reported in the near future.

Although fluoride materials are generally expected to be moisture sensitive, the quaternary fluorides, $Na_4MU_6F_{30}$ (M = Mn^{2+}, Co^{2+}, Ni^{2+}, Cu^{2+}, and Zn^{2+}), are in fact air and moisture stable for at least several months and, surprisingly, are insoluble even in concentrated nitric acid.

Structure. The family of compounds, $Na_4MU_6F_{30}$ (M = Mn^{2+}, Co^{2+}, Ni^{2+}, Cu^{2+}, and Zn^{2+}), crystallizes in the trigonal space group $P\bar{3}c1$ and exhibits a complex three-dimensional crystal structure consisting of corner- and edge-shared UF_9 and MF_6 polyhedra (see Figure 2).

The three-dimensional framework has an overall composition of $MU_6F_{30}^{4-}$ and is charge balanced by four Na^+ cations. The most basic building units of the framework are corner- and edge-shared UF_9 polyhedra that arrange into U_2F_{16} dimers that further assemble into one-dimensional chains oriented along the *c*-axis via corner- or edge- sharing between the U_2F_{16} dimers (see Figure 3). These chains are connected to each other via corner-sharing in the *ab*-plane, forming the anionic $U_6F_{30}^{6-}$ uranium−fluorine building block. The most interesting feature of this structure is the presence of large and small hexagonal channels oriented along the *c*-axis created by the arrangement of the $U_6F_{30}^{6-}$ building blocks. The large hexagonal channel consists of corner- and edge-shared UF_9 polyhedra, and the

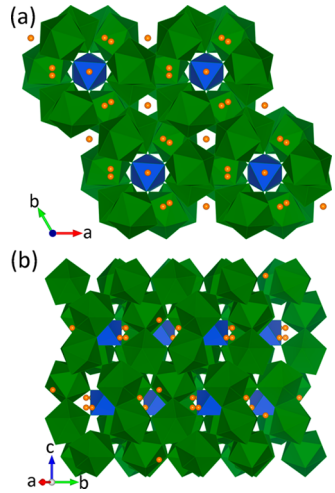

Figure 2. Illustration of the polyhedral structure representation of $Na_4MU_6F_{30}$ along the (a) *c*- and (b) *a*-axis. The three-dimensional framework consisting of corner- or edge-sharing UF_9 and MF_6 polyhedra is shown. The green, blue, and orange spheres/polyhedra represent U^{4+}, M^{2+}, and Na^+ ions, respectively.

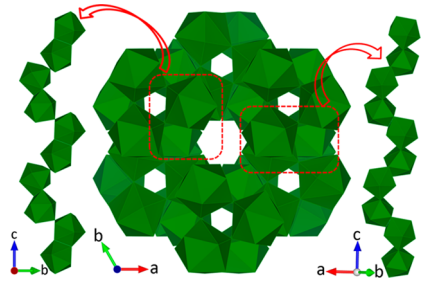

Figure 3. Polyhedral structure representation emphasizing the connectivities of the UF_9 polyhedra and illustrating the resulting hexagonal channels. The linear chains are linked together in the *ab*-plane to form the hexagonal channels, where the large hexagonal channel is surrounded by six small hexagonal channels.

MF_6 octahedra and $Na(2)^+$ cations reside in an alternating arrangement in the channel interior. This channel structure is further connected to other U^{4+} cations in the *ab*-plane and is surrounded by the six small hexagonal channels as seen in Figures 3 and 4a. The small hexagonal channel is composed of corner- and edge-shared UF_9 polyhedra and contains the $Na(1)^+$ cations. Two sets of three corner-shared UF_9 polyhedra lie in a trigonal antiprismatic position creating three-membered rings, which are further connected by three UF_9 polyhedra via edge-sharing (see Figure 4b).

The U^{4+} cation is located in a distorted monocapped square antiprismatic coordination environment with U−F bond lengths of 2.226(6)−2.428(4) Å. The M^{2+} cations are coordinated by six fluorine atoms forming a nearly regular octahedron with M−F bond distances of 1.986(5)−2.056(5) Å. The bond lengths vary for the different transition-metal cations and are listed in Table 2. The six fluorine atoms around the MF_6 polyhedra are further linked to six uranium cations. The local coordination environments of the U^{4+} and M^{2+} cations are shown in Figure 5. There are three crystallographically unique sodium cations, Na(1) located in the small channel, Na(2) located in the large channel, and Na(3) located within the framework but not in any channel. The Na(3) atoms are disordered over two sites that are 1.11(3) Å apart from each

dx.doi.org/10.1021/ja412725r | J. Am. Chem. Soc. 2014, 136, 3955−3963

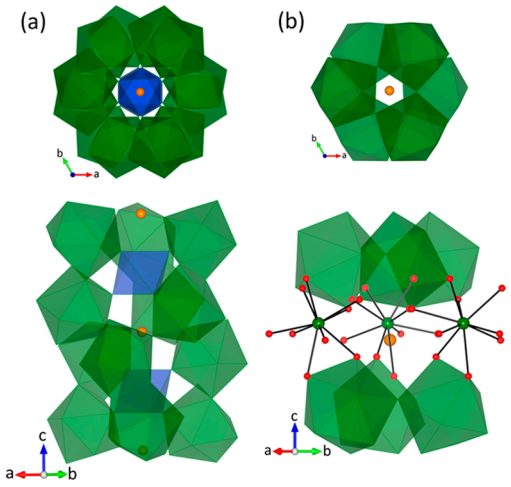

Figure 4. Illustration of the representative portion of the large and small hexagonal channels in $Na_4MU_6F_{30}$. The Na(2) atoms and the MF_6 polyhedra reside alternately in the channel, whereas only Na(1) atoms occupy inside of the smaller channels, as illustrated in (a) and (b), respectively. The green, blue, and orange spheres/polyhedra represent U^{4+}, M^{2+}, and Na^+ ions, respectively.

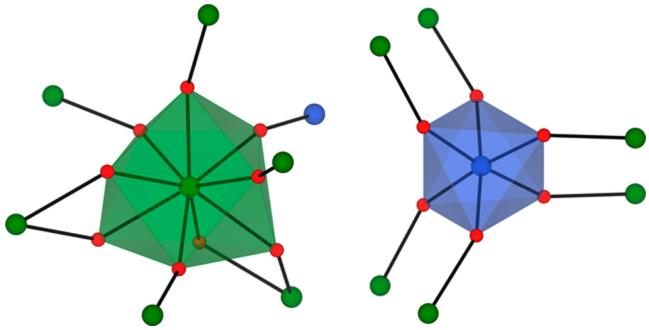

Figure 5. Representation of the local coordination environments of the U^{4+} and M^{2+} cations, and the connectivity to other metal cations around the polyhedra. The U^{4+} cation is found in a monocapped distorted square prism, and the M^{2+} cation exhibits a nearly regular octahedron.

other. All the sodium cations are found in irregular coordination environments with Na–F distances ranging from 2.262(5) to 2.725(5) Å. Bond valence sum[42,43] calculation resulted in values of 0.9 −1.19, 2.03–2.19, and 4.12–4.15 for Na^+, M^{2+}, and U^{4+}, respectively, supporting the +4 oxidation state of the uranium in the crystal structures.

A plot of the unit cell parameters of $Na_4MU_6F_{30}$ (M = Mn^{2+}, Co^{2+}, Ni^{2+}, Cu^{2+}, and Zn^{2+}) along with the ionic radii of the respective divalent transition element in an octahedral coordination environment is shown in Figure 6. The change of the *a*-axis length is in good agreement with the trend observed for the M^{2+} ionic radii.[44] By comparison, the lengths of the *c*-axes remain relatively constant. This is likely due to the presence of the corner-shared UF_9 polyhedra in the *ab*-plane, whereas corner- and edge-sharing connectivity is found along the *c*-axis. The absence of the edge-sharing between the UF_9 polyhedra in the *ab*-plane may provide more flexibility for the *a*-axis to adjust to accommodate the size of the different transition elements, compared to the *c*-axis containing edge sharing. One might expect that the size of the large hexagonal channel can adjust itself to accommodate other metal octahedra in different oxidation states, such as an FeF_6^{3-} octahedron,

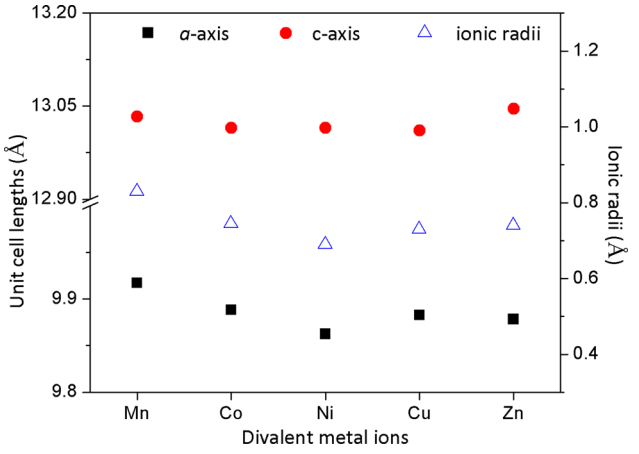

Figure 6. The plot of the unit cell parameters for $Na_4MU_6F_{30}$ (M = Mn, Co, Ni, Cu, and Zn) along with the ionic radii for the respective transition element found in the octahedral coordination environment.

similar in size to the divalent transition elements reported here. The charge balance would have to be achieved by decreasing the number of sodium cations.

Among the M^{2+} cations found in the reported series, Cu^{2+} (d^9) is the transition-metal cation known to undergo a Jahn–Teller (J–T) distortion.[45] In general, the octahedrally coordinated Cu^{2+} cation undergoes a tetragonal distortion where the octahedra are typically elongated or compressed along the four-fold axis.[46–49] Although the F–Cu–F angles (averaged angles: 90.1° and 173.7°) in $Na_4CuU_6F_{30}$ are slightly distorted from the regular octahedron (90° and 180°), the material exhibits six equivalent Cu–F bond distances (6 × 1.995(4) Å), indicating the lack of a measurable distortion. There are few examples, such as $[Cu(XeF_2)_6](SbF_6)_2$ and $[M(H_2O)_6]SiF_6$ (M = Cr^{2+}, Cu^{2+}), that were reported to exhibit an undistorted CuX_6 (X = F^-, O^{2-}) octahedron in the crystal structure.[50,51] It is reasonable to assume that in some cases the J–T effect might be suppressed because of the symmetry and rigidity of the crystal structure.[52] EXAFS studies, however, often revealed that the Cu^{2+} cations in regular octahedra do in fact undergoes a J–T distortion through a dynamic J–T effect as a function of temperature.[53–55] We would note that our single crystal data were collected at two temperatures (100 and 298 K) and are almost identical as seen in Tables 1, 2, S2, and S3, providing no indication of a change in the copper coordination environment as a function of temperature. We examined the anisotropic displacement parameters (ADPs) for the CuF(4) octahedron, resulting in the quite similar U_3/U_1 values of 1.77 and 1.69 (100 and 298 K) for the F(4) atom. This is shown in Figure S3, where quite spherical thermal ellipsoids are found, and no evidence for unusual distortions, such as a dynamic distortion along the Cu–F(4) bond, is observed. We also performed a mean square displacement amplitude analysis because this method is a much more sensitive way of detecting any dynamic disorder along the metal–ligand bond than the thermal ellipsoid analysis. Using the program THMA11[53,56] equipped on a Wingx crystallographic software package,[57] very similar $\langle d^2 \rangle$ values (× 10^4 Å) of 72(16) and 86(13) (100 and 298 K) for the Cu–F(4) bond were obtained, which again suggests that no significant dynamic disorder is taking place in the Cu–F(4) polyhedron down to at least 100 K. The EPR data collected at room temperature are shown in Figure 7, where no obvious disorder, such as a

dx.doi.org/10.1021/ja412725r | J. Am. Chem. Soc. 2014, 136, 3955–3963

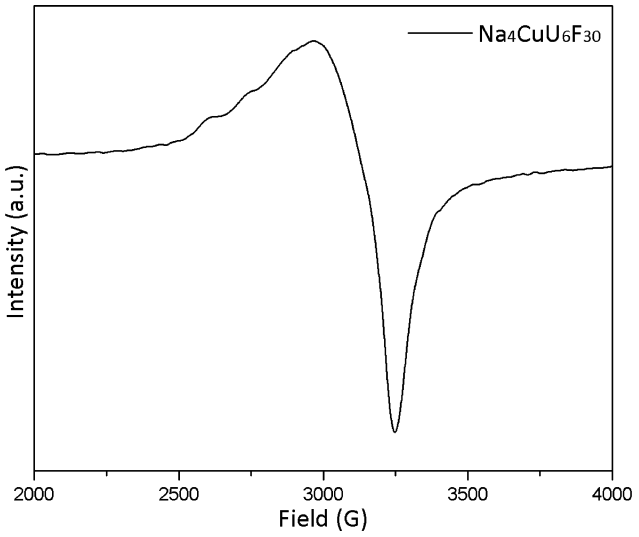

Figure 7. The EPR spectrum for $Na_4CuU_6F_{30}$ collected at room temperature.

tetragonal elongation through a dynamic distortion, was detected. From these analyses it appears that the Cu^{2+} cation in $Na_4CuU_6F_{30}$ exhibits an unusual coordination environment that, at least between 100 and 298 K, lacks the normal J−T distortion. Nonetheless, future EXAFS experiments to examine $Na_4CuU_6F_{30}$ for the existence of a dynamic J−T distortion are planned.

UV−vis Diffuse Reflectance Spectroscopy. UV−vis diffuse reflectance data were collected on ground crystals of the reported materials, $Na_4MU_6F_{30}$ (M = Mn^{2+}, Co^{2+}, Ni^{2+}, Cu^{2+}, and Zn^{2+}). Reflectance data were converted to absorbance using the Kubelka−Munk function.[41] As seen in Figure 8, all spectra are similar to each other, containing several absorption bands that are mainly attributed to the f−f transitions in the U^{4+} cation. Although d−d transitions from the divalent transition elements are present, the transitions are not prominent in the spectra. This is likely due to the very strong and sharp f−f transitions that obscure the absorption

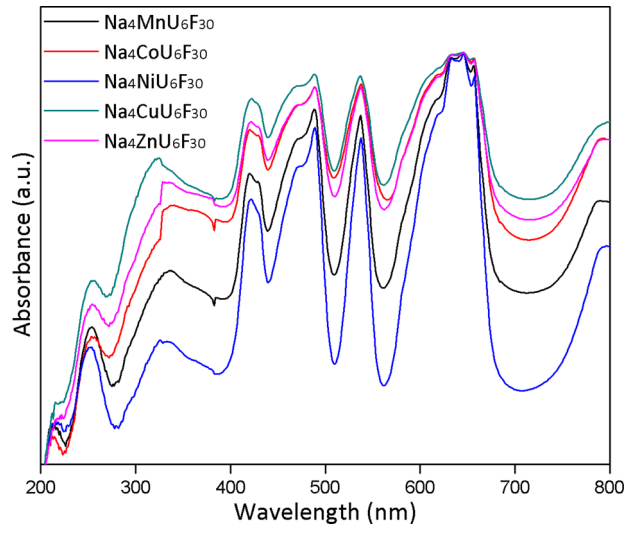

Figure 8. UV−vis diffuse absorbance spectroscopy data for $Na_4MU_6F_{30}$ (M = Mn, Co, Ni, Cu, and Zn). The absorption bands above 400 nm are attributed to the f−f transitions in the U^{4+} cation.

bands from the d−d transitions. The observed bands above 400 nm include the f−f transitions of the U^{4+} cation from the ground state of $^3H_4$ to several excited states, which is consistent with previously known materials, confirming the presence of U^{4+}.[32,33] The band gaps were estimated by the onset of the absorption edges and yield values of ∼4.1 eV for all five fluorides, indicating insulating behavior.

Thermal Behavior. The thermal behavior of the reported materials was investigated by heating the ground crystals in air in a TGA followed by PXRD analysis of the resultant products. Although the formation of oxide materials was expected from heating these quaternary fluorides in air, the experiment was performed to determine if the fluorides could be converted to a single-phase oxide material. In all cases, however, the X-ray diffraction patterns of the samples heated to 800 °C in air consisted of $Na_2U_2O_7$[58] and MU_3O_{10}[59] as the major products and at least one additional unidentified minor product, indicating that the thermal treatment decomposed the fluorides to give a mixtures of several U^{6+}-containing oxide materials. The powder X-ray patterns of the products after heating are given in Figure S4.

Magnetic Properties. The magnetic properties of these quaternary fluorides containing U^{4+} and M^{2+} were investigated since both U^{4+} ($5f^2$) and M^{2+} = Mn ($3d^5$), Co ($3d^7$), Ni ($3d^8$), Cu ($3d^9$) contain unpaired electrons. Only for the Zn^{2+}-containing fluoride, $Na_4ZnU_6F_{30}$, was the uranium the sole contributor to the magnetic susceptibility; for the other compositions, the measured magnetic susceptibility reflected the sum of the U^{4+} and M^{2+} contributions.

The temperature dependence of the magnetic susceptibility data for $Na_4ZnU_6F_{30}$ measured in an applied field of 1000 Oe is shown in Figure 9, with the inset showing the inverse

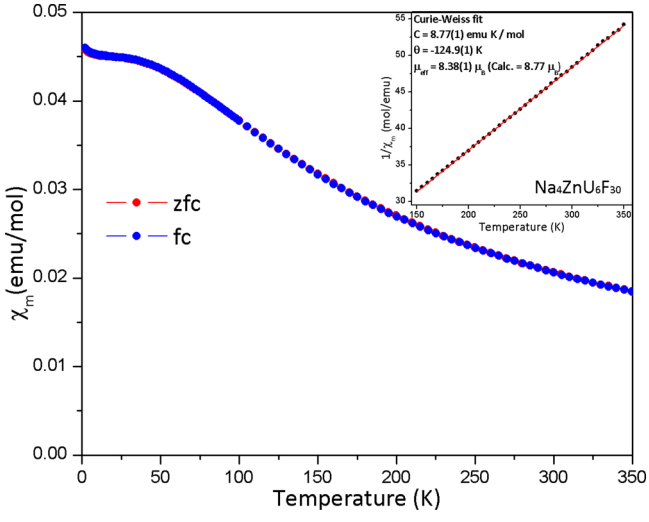

Figure 9. Temperature dependence of the molar magnetic susceptibility of $Na_4ZnU_6F_{30}$ measured in an applied field of 1000 Oe. The red solid line in the inset represents the C−W fit of the data.

susceptibility versus temperature plot. No differences are observed between ZFC and FC data. The inverse susceptibility data in the linear high temperature range (150−350 K) were fitted to the Curie−Weiss (C−W) law, $\chi = C/(T - \theta)$, where C is the Curie and θ is the Weiss constant. The constants extracted from the fit are summarized in Table 3. An effective magnetic moment of 3.42 μ_B was obtained for the U^{4+} cation, consistent with the theoretical value of 3.58 μ_B, calculated using

dx.doi.org/10.1021/ja412725r | J. Am. Chem. Soc. 2014, 136, 3955−3963

Table 3. Constants Extracted from the Magnetic Susceptibility Data for $Na_4MU_6F_{30}$ (M = Mn^{2+}, Co^{2+}, Ni^{2+}, Cu^{2+}, and Zn^{2+}). C, θ, and μ_{eff} Represent the Curie and Weiss Constants and Effective the Magnetic Moment, Respectively

				$\mu_{eff}(M^{2+})/\mu_B$ at 2 K	
	C (emu·K/mol)	θ (K)	combined μ_{eff}/μ_B	observed	expected
$Na_4MnU_6F_{30}$	13.1(1)	−68.4(2)	10.2(1)	5.48	5.92
$Na_4CoU_6F_{30}$	12.1(1)	−79.6(2)	9.84(1)	3.96	3.87
$Na_4NiU_6F_{30}$	9.83(1)	−98.9(1)	9.21(1)	2.79	2.83
$Na_4CuU_6F_{30}$	9.03(1)	−101.6(1)	8.94(1)	2.13	1.73
$Na_4ZnU_6F_{30}$	8.77(1)	−124.9(1)	8.38(1)	–	–

full Russell−Saunders coupling for a $^3H_4$ ground state. The magnetic susceptibility starts to deviate from the C−W law for temperatures below 150 K, indicating the loss of thermally accessible excited states of the uranium and the formation of a singlet ground state. The stabilization of the U^{4+} ($5f^2$) singlet ground state at low temperature is consistent with what has been observed in other U^{4+}-containing materials.[60−62]

The temperature dependence of the susceptibility data for $Na_4MU_6F_{30}$ (M = Mn^{2+}, Co^{2+}, Ni^{2+}, and Cu^{2+}) collected in an applied field of 1000 Oe is shown in Figures 10 and S5−S7,

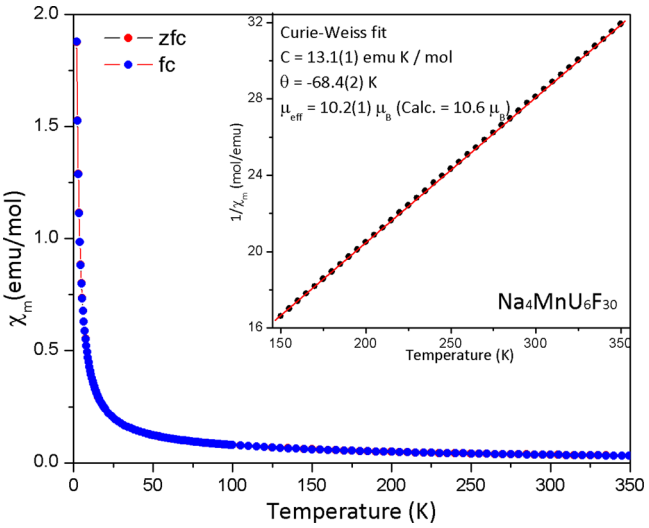

Figure 10. Temperature dependence of the molar magnetic susceptibility for $Na_4MnU_6F_{30}$ measured in an applied field of 1000 Oe. The red solid line in the inset represents the C−W fit of the data.

with the inset showing the inverse susceptibility versus temperature plot. The noticeable difference in the low temperature susceptibility of these data, compared to what is observed in the Zn-containing sample, is due to the additional paramagnetic contributions from the divalent transition elements. Nonetheless, the magnetic susceptibilities all deviate from the C−W law at intermediate temperatures (50−150 K) as the uranium's excited states become depopulated. At the lowest temperatures, only the paramagnetic transition metal cations contribute to the magnetic moment. The high temperature regions of the inverse susceptibility data (150−350 K) were fitted to the C−W law, and the values obtained from the fit are listed in Table 3. In all cases, the effective magnetic moments are close to the moments calculated from the sum of the U^{4+} and M^{2+} contributions. The magnetic moment per U^{4+} calculated from the $Na_4MnU_6F_{30}$ data (μ_{eff}/Mn^{2+} = 5.92 μ_B) is 3.39 μ_B, which is slightly smaller than the theoretical value of 3.58 μ_B, however, it is in good agreement with the value extracted from $Na_4ZnU_6F_{30}$ (μ_{eff}/U^{4+} = 3.42 μ_B) (see Table 3).

The low temperature magnetic susceptibility of these fluorides is expected to originate solely on the paramagnetic divalent cations because the U^{4+} cation exhibits a nonmagnetic singlet ground state at low temperature and hence has no moment to contribute. Figure S8 shows the temperature dependence of the $\chi_m T$ data for $Na_4MU_6F_{30}$ (M = Mn^{2+}, Co^{2+}, Ni^{2+}, and Cu^{2+}). The magnetic moment extracted from the data at 2 K yields effective magnetic moments of 5.48, 3.96, 2.79, and 2.13 μ_B, for Mn^{2+}, Co^{2+}, Ni^{2+}, and Cu^{2+}, respectively, which compares well with their expected spin-only magnetic moments of 5.92, 3.87, 2.83, and 1.73 μ_B. This confirms that the magnetic contributions are almost entirely due to the divalent transition elements at low temperature. This phenomenon is also well supported by the magnetization as a function of applied magnetic field measured at 2 K for $Na_4MnU_6F_{30}$. The data are plotted in Figure 11 and are in good agreement with the theoretical behavior for the Mn^{2+} cation calculated from the Brillouin function for a spin of 5/2.[63]

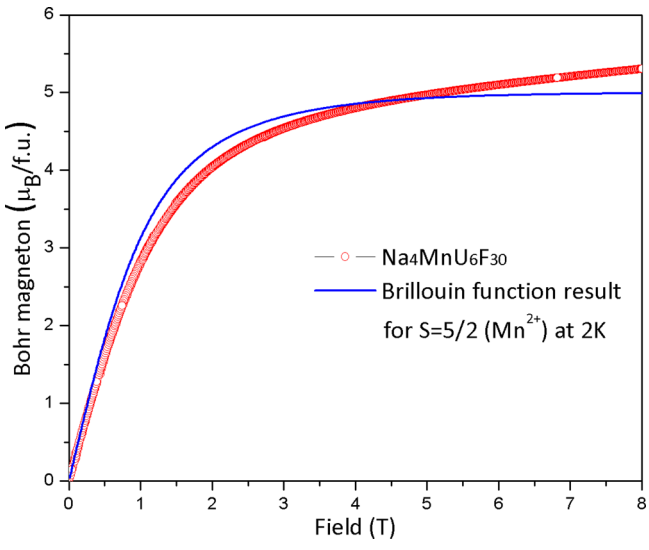

Figure 11. The field dependence of the magnetic moment of $Na_4MnU_6F_{30}$ measured at 2 K along with the theoretical behavior for the Mn^{2+} cation calculated from the Brillouin function for a spin of 5/2.

For all compositions studied, local magnetic interactions are not well supported, and no evidence for any long-range magnetic ordering was observed down to 2 K, implying the materials exhibit single ion type behavior due to the well isolated M^{2+} sites. It has been shown previously for materials containing U^{4+} that the Weiss temperature reflects the temperature driven gap between the triplet and singlet

dx.doi.org/10.1021/ja412725r | J. Am. Chem. Soc. 2014, 136, 3955−3963

state.[60−62,64−66] However, here we present a series of isotypic U−F frameworks that host nonmagnetic and paramagnetic transition metal cations. We note that there is a significant change of the Weiss temperatures along the series, see Table 3 and Figure 12. Furthermore, an interesting trend appears

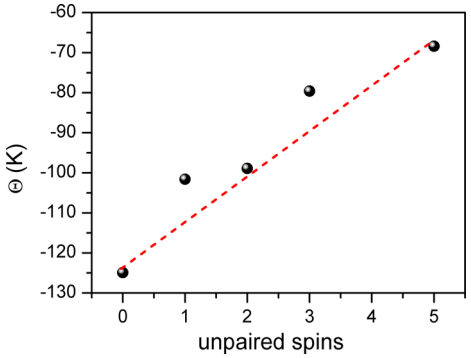

Figure 12. A plot of the Weiss constant as a function of the number of unpaired spins on the divalent transition-metal ions in $Na_4MU_6F_{30}$ (M = Mn^{2+}, Co^{2+}, Ni^{2+}, Cu^{2+}, and Zn^{2+}). The dashed red line is included to guide the eye.

revealing the dependence of the Weiss temperatures by almost a factor of 2 on the number of unpaired electrons of the M^{2+} cations as seen in Figure 12. The deviation from the linear trend for the Co^{2+} and Cu^{2+} cations is not entirely unexpected considering their more anisotropic character compared to the other cations.[67] The magnetic characteristics of the series are related to inherent properties of the single ion anisotropies, as any magnetic exchange interactions between the M^{2+} cations would vanish due to the nonmagnetic ground state of the U^{4+} cation, leaving dipolar interactions of the M^{2+} cations as the only source for magnetic ordering. In order to better understand the magnetic interactions between f- and d-orbitals, the $\chi_mT(M) - \chi_mT(Zn)$ (M = Mn^{2+}, Co^{2+}, Ni^{2+}, and Cu^{2+}) data are plotted as a function of temperature, which method was previously utilized in other literature.[68] In this case, the χ_mT data for $Na_4ZnU_6F_{30}$ shown in Figure 13 were used as a reference because it contains the U^{4+} as a sole magnetic contributor. As shown in Figure 14, the $\chi_mT(M) - \chi_mT(Zn)$

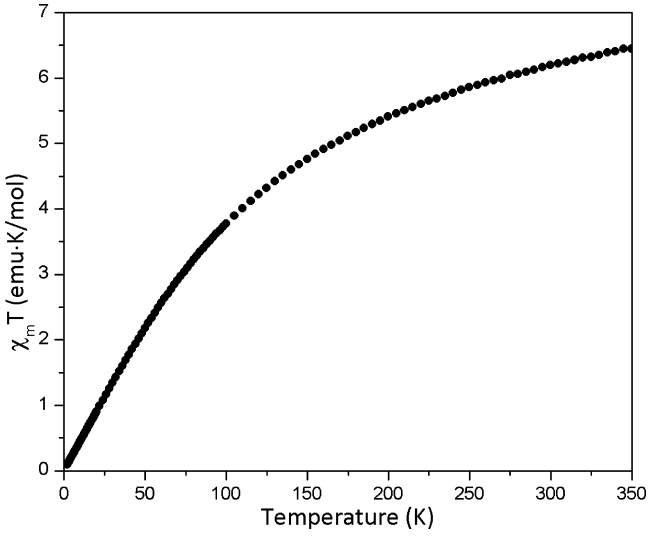

Figure 13. Plot of χ_mT vs temperature (K) for $Na_4ZnU_6F_{30}$.

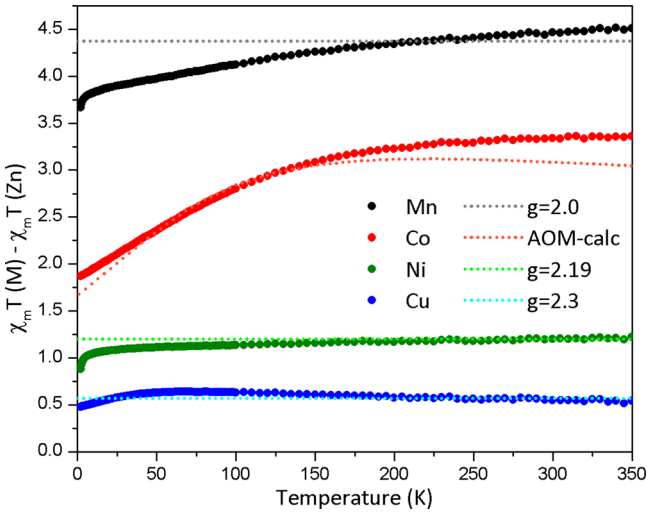

Figure 14. A plot of the temperature dependence of the $\chi_mT(M) - \chi_mT(Zn)$ (M = Mn^{2+}, Co^{2+}, Ni^{2+}, and Cu^{2+}) data. The dotted lines represent the theoretical single ion behavior for the respective metal cations. For Co^{2+}, the atomic overlap model was utilized.

data follow the theoretical single ion behavior (dotted lines). For the Co^{2+} ion the angular overlap model was utilized because of spin−orbit coupling and quartet ground state of the Co^{2+} ion.[69,70] Among this series, the unpaired electrons in the t_{2g} orbitals on the Mn^{2+} and Co^{2+} cations have a more pronounced influence on the gap between the triplet and singlet states of the U^{4+} cation.

CONCLUSIONS

We have synthesized and characterized a new series of quaternary fluorides containing U^{4+}, $Na_4MU_6F_{30}$ (M = Mn^{2+}, Co^{2+}, Ni^{2+}, Cu^{2+}, and Zn^{2+}). The U^{6+} in the uranium starting material was successfully reduced to U^{4+} using a mild hydrothermal route. The materials exhibit a complex three-dimensional crystal structure, in which the U^{4+} cation is found in a nine-fold coordination environment. The Cu^{2+} in $Na_4CuU_6F_{30}$ is located in an undistorted octahedral coordination environment, suggesting the absence of an observable J−T distortion. From the temperature and field-dependent magnetic measurements it was confirmed that the magnetic U^{4+} exhibits a nonmagnetic singlet ground state at low temperature. No long-range magnetic order was observed for any of the five compositions above 2 K.

ASSOCIATED CONTENT

Supporting Information

X-ray data in CIF format, powder XRD patterns, EPR spectroscopic data, magnetic property data, and crystallographic data for $Na_4CuU_6F_{30}$ collected at 298 K. These materials are free of charge via the Internet at http://pubs.acs.org.

AUTHOR INFORMATION

Corresponding Author

zurloye@mailbox.sc.edu

Notes

The authors declare no competing financial interest.

■ ACKNOWLEDGMENTS

Research supported by the U.S. Department of Energy, Office of Basic Energy Sciences, Division of Materials Sciences and Engineering under award DE-SC0008664. Magnetic measurements were performed at the University of Houston and support from the National Science Foundation under award DMR-1149899 is gratefully acknowledged. We also thank Dr. Thomas Makris for help collecting the room temperature EPR data.

■ REFERENCES

(1) Burns, P. C.; Olson, R. A.; Finch, R. J.; Hanchar, J. M.; Thibault, Y. *J. Nucl. Mater.* **2000**, *278*, 290.
(2) Jackson, J. M.; Burns, P. C. *Can. Mineral.* **2001**, *39*, 187.
(3) Kim, K.-T. *J. Nucl. Mater.* **2010**, *404*, 128.
(4) Ling, J.; Morrison, J. M.; Ward, M.; Poinsatte-Jones, K.; Burns, P. C. *Inorg. Chem.* **2010**, *49*, 7123.
(5) Oji, L. N.; Martin, K. B.; Stallings, M. E.; Duff, M. C. *Nucl. Technol.* **2006**, *154*, 237.
(6) Yamaji, A.; Nakano, Y.; Uchikawa, S.; Okubo, T. *Nucl. Technol.* **2012**, *179*, 309.
(7) Andriychuk, V. *J. Energy Power Eng.* **2011**, *5*, 1126.
(8) Ladeira, A. C. Q.; Goncalves, J. S.; Morais, C. A. *Environ. Technol.* **2011**, *32*, 127.
(9) McNamara, B.; Scheele, R.; Kozelisky, A.; Edwards, M. *J. Nucl. Mater.* **2009**, *394*, 166.
(10) Morel, B.; Duperret, B. *J. Fluorine Chem.* **2009**, *130*, 7.
(11) Vanderhaegen, M.; Janssens-Maenhout, G.; Peerani, P.; Poucet, A. *Nucl. Eng. Des.* **2010**, *240*, 2988.
(12) Penneman, R. A.; Ryan, R. R.; Rosenzweig, A. *Struct. Bonding (Berlin)* **1973**, *13*, 1.
(13) Cousson, A.; Tabuteau, A.; Pages, M.; Gasperin, M. *Acta Crystallogr., Sect. B* **1979**, *B35*, 1198.
(14) Rosenzweig, A.; Ryan, R. R.; Cromer, D. T. *Acta Crystallogr., Sect. B* **1973**, *29*, 460.
(15) Schmidt, R.; Mueller, B. G. *Z. Anorg. Allg. Chem.* **2004**, *630*, 2393.
(16) Zachariasen, W. H. *Acta Crystallogr.* **1948**, *1*, 265.
(17) Zachariasen, W. H. *Acta Crystallogr.* **1954**, *7*, 792.
(18) Vedrine, A.; Trottier, D.; Cousseins, J. C.; Chevalier, R. *Mater. Res. Bull.* **1979**, *14*, 583.
(19) Vedrine, A.; Baraduc, L.; Cousseins, J. C. *Mater. Res. Bull.* **1973**, *8*, 581.
(20) Severance, R. C.; Cortese, A. J.; Smith, M. D.; zur Loye, H.-C. *J. Chem. Crystallogr.* **2013**, *43*, 171.
(21) Severance, R. C.; Vaughn, S. A.; Smith, M. D.; zur Loye, H.-C. *Solid State Sci.* **2011**, *13*, 1344.
(22) Severance, R. C.; Smith, M. D.; zur Loye, H.-C. *Inorg. Chem.* **2011**, *50*, 7931.
(23) Tian, T.; Yang, W.; Wang, H.; Dang, S.; Pan, Q.-J.; Sun, Z.-M. *Inorg. Chem.* **2013**, *52*, 7100.
(24) Wu, H.-Y.; Yang, X.-y.; Li, Y.-h.; Yang, W. *Inorg. Chem. Commun.* **2012**, *23*, 46.
(25) Wang, J.-L.; Deng, Z.-Y.; Duan, S.-B.; Xing, Y.-H. *J. Coord. Chem.* **2012**, *65*, 3546.
(26) Siidra, O. I.; Nazarchuk, E. V.; Krivovichev, S. V. *Eur. J. Inorg. Chem.* **2012**, *2012*, 194.
(27) Lee, C.-S.; Lin, C.-H.; Wang, S.-L.; Lii, K.-H. *Angew. Chem., Int. Ed.* **2010**, *49*, 4254.
(28) Vlaisavljevich, B.; Diaconescu, P. L.; Lukens, W. L., Jr.; Gagliardi, L.; Cummins, C. C. *Organometallics* **2013**, *32*, 1341.
(29) Fortier, S.; Kaltsoyannis, N.; Wu, G.; Hayton, T. W. *J. Am. Chem. Soc.* **2011**, *133*, 14224.
(30) Schnaars, D. D.; Wu, G.; Hayton, T. W. *J. Am. Chem. Soc.* **2009**, *131*, 17532.
(31) Fortier, S.; Melot, B. C.; Wu, G.; Hayton, T. W. *J. Am. Chem. Soc.* **2009**, *131*, 15512.
(32) Yeon, J.; Smith, M. D.; Sefat, A. S.; zur Loye, H.-C. *Inorg. Chem.* **2013**, *52*, 2199.
(33) Yeon, J.; Smith, M. D.; Sefat, A. S.; Tran, T. T.; Halasyamani, P. S.; zur Loye, H.-C. *Inorg. Chem.* **2013**, *52*, 8303.
(34) Yeon, J.; Sefat, A. S.; Tran, T. T.; Halasyamani, P. S.; zur Loye, H.-C. *Inorg. Chem.* **2013**, *52*, 6179.
(35) Cochell, T.; Manthiram, A. *Langmuir* **2012**, *28*, 1579.
(36) Piao, X.; Machida, K.-i.; Horikawa, T.; Yun, B. *J. Lumin.* **2009**, *130*, 8.
(37) Kumar, L. H.; Viswanathan, B.; Murthy, S. S. *J. Alloys Compd.* **2008**, *461*, 72.
(38) *SMART version 5.630, SAINT+ version 6.45, and SADABS version 2.10*; Bruker Analytical X-ray Systems, Inc.: Madison, WI, 2003.
(39) Dolomanov, O. V.; Bourhis, L. J.; Gildea, R. J.; K., H. A.; Puschmann, H. *J. Appl. Crystallogr.* **2009**, *42*, 339.
(40) Sheldrick, G. M. *Acta Crystallogr.* **2008**, *A64*, 112.
(41) Kubelka, P.; Munk, F. Z. *Tech. Phys.* **1931**, *12*, 593.
(42) Brese, N. E.; O'Keeffe, M. *Acta Crystallogr.* **1991**, *B47*, 192.
(43) Brown, I. D.; Altermatt, D. *Acta Crystallogr.* **1985**, *B41*, 244.
(44) Shannon, R. D.; Prewitt, C. T. *Acta Crystallogr., Sect. B* **1969**, *25*, 925.
(45) Jahn, H. A.; Teller, E. *Proc. R. Soc. London, Ser. A* **1937**, *161*, 220.
(46) Stratemeier, H.; Wagner, B.; Krausz, E. R.; Linder, R.; Schmidtke, H. H.; Pebler, J.; Hatfield, W. E.; ter, H. L.; Reinen, D.; Hitchman, M. A. *Inorg. Chem.* **1994**, *33*, 2320.
(47) Tucker, D. A.; White, P. S.; Trojan, K. L.; Kirk, M. L.; Hatfield, W. E. *Inorg. Chem.* **1991**, *30*, 823.
(48) Wood, J. S.; Keijzers, C. P.; De, B. E.; Buttafava, A. *Inorg. Chem.* **1980**, *19*, 2213.
(49) Joesten, M. D.; Takagi, S.; Lenhert, P. G. *Inorg. Chem.* **1977**, *16*, 2680.
(50) Tavcar, G.; Goreshnik, E.; Mazej, Z. *J. Fluorine Chem.* **2006**, *127*, 1368.
(51) Ray, S.; Zalkin, A.; Templeton, D. H. *Acta Crystallogr., Sect. B* **1973**, *29*, 2748.
(52) Cotton, F. A.; Daniels, L. M.; Murillo, C. A.; Quesada, J. F. *Inorg. Chem.* **1993**, *32*, 4861.
(53) Halcrow, M. A. *Dalton Trans.* **2003**, 4375.
(54) Persson, I.; Persson, P.; Sandstroem, M.; Ullstroem, A.-S. *J. Chem. Soc., Dalton Trans.* **2002**, 1256.
(55) Burns, P. C.; Hawthorne, F. C. *Can. Mineral.* **1996**, *34*, 1089.
(56) Blackburn, A. C.; Gallucci, J. C.; Gerkin, R. E. *Acta Crystallogr., Sect. C* **1991**, *C47*, 2019.
(57) Farrugia, L. J. *J. Appl. Crystallogr.* **1999**, *32*, 837.
(58) Gasperin, M. *J. Less-Common Met.* **1986**, *119*, 83.
(59) Miyake, C.; Kondo, T.; Takamiya, T.; Yoneda, Y. *J. Alloys Compd.* **1993**, *193*, 116.
(60) Siladke, N. A.; Meihaus, K. R.; Ziller, J. W.; Fang, M.; Furche, F.; Long, J. R.; Evans, W. J. *J. Am. Chem. Soc.* **2011**, *134*, 1243.
(61) Nocton, G.; Pecaut, J.; Mazzanati, M. *Angew. Chem., Int. Ed.* **2008**, *47*, 3040.
(62) Schelter, E. J.; Morris, D. E.; Scott, B. L.; Thompson, J. D.; Kiplinger, J. L. *Inorg. Chem.* **2007**, *46*, 5528.
(63) Darby, M. I. *Br. J. Appl. Phys.* **1967**, *18*, 1415.
(64) Lai, Y.-L.; Chiang, R.-K.; Lii, K.-H.; Wang, S.-L. *Chem. Mater.* **2008**, *20*, 523.
(65) Wang, C.-M.; Liao, C.-H.; Chen, P.-L.; Lii, K.-H. *Inorg. Chem.* **2006**, *45*, 1436.
(66) Almond, P. M.; Deakin, L.; Mar, A.; Albrecht-Schmitt, T. E. *J. Solid State Chem.* **2001**, *158*, 87.
(67) Kahn, O. *Molecular Magnetism*; VCH: New York, 1993.
(68) Rinehart, J. D.; Harris, T. D.; Kozimor, S. A.; Bartlett, B. M.; Long, J. R. *Inorg. Chem.* **2009**, *48*, 3382.
(69) Gerloch, M. *Magnetism and Ligand Field Theory*; Cambridge University Press: Cambridge, U.K., 1983.
(70) Gerloch, M.; McMeeking, R. F. *J. Chem. Soc., Dalton Trans.* **1975**, 2443.